Optics Letters

Dual resonance akinetic dispersive cavity swept source at 900 kHz using a cFBG and an intensity modulator

Rene Riha,* Adrian Bradu, and Adrian Podoleanu

Applied Optics Group, School of Physical Sciences, University of Kent, Canterbury, Kent, CT2 7NH, UK
**Corresponding author: rr406@kent.ac.uk*

Received 12 May 2022; revised 6 July 2022; accepted 9 July 2022; posted 11 July 2022; published 4 August 2022

In this paper, a fast dual resonance akinetic optical swept source operating at 1550 nm is demonstrated. Instead of modulating the optical amplifier gain reported in our previous studies, here we employ a fiber intensity modulator as a mode-locking element. A chirped fiber Bragg grating is used to provide sufficient dispersion in the laser cavity. A tuning range of 25 nm is obtained for a sweep frequency of ≈900 kHz with a 6-dB drop-off in sensitivity at 2.6-mm optical path difference.

https://doi.org/10.1364/OL.463675

Introduction. Optical coherence tomography (OCT) is a non-invasive, non-contact imaging technique based on low-coherence interferometry [1,2]. The essential parameters determining the OCT performance are the axial resolution, imaging range, and speed, as well as the sensitivity drop-off with imaging depth. One of the OCT methods that in the last decade has proven MHz sweep rates is the swept source (SS)-OCT [3]. This allows not only a high speed, but a larger axial range than the spectrometer based-OCT method.

Several operation principles for fast wavelength tuning have been demonstrated. The most widely used mechanical solutions employ Fabry–Perot tunable filters [4,5], polygon mirror scanners [6], or tunable micro-electromechanical systems (MEMS) together with an optical amplifier [7]. Akinetic wavelength-swept source lasers (AKSS) with an integrated semiconductor opto-electronic design at central wavelengths of 1060, 1310, and 1550 nm [8,9] have been reported recently. Akinetic wavelength tuning based on an active mode-locking (AML) method of a dispersive cavity [10,11] has also been reported.

Previously, we have reported on mode-locked dispersive cavity lasers for SS-OCT systems based on the so-called dual resonance sweeping regime. Several configurations implementing this regime were demonstrated at 850 and 1550 nm [12,13]. In these reports, sweep frequencies close to 1 MHz were achieved in long length cavities, where otherwise conventional AKSS configurations would allow only a few-kHz sweeping rate. One commonly used approach to increase the sweep frequency is to reduce the cavity length [11,14].

In the previous reports on the dual resonance regime, mode-locking was achieved by modulating the gain of the semiconductor optical amplifier (SOA) in the laser cavity. A first drawback of modulating the gain originates from the nonlinear operation of SOA chips, where both the optical power and the spectral bandwidth depend on the value of the driving current. For a more stable tuning, it would be preferable to operate the SOA at a constant injection current. A second drawback is due to the frequency limitation of commercial SOAs, where their surrounding electronics circuitry does not accept direct current modulation at GHz rates. For a more stable tuning, it is also preferable to operate with modulation frequencies larger than 1 GHz [10]. In the present study, the optical amplification is separated from the mode-locking mechanism by employing an additional component, an intensity modulator, responsible for the mode-locking of the optical field in the cavity only. Intensity modulators can operate at frequencies in excess of 10 GHz.

Methods and results. The AKSS researched is depicted in Fig. 1. The setup uses an SOA as a gain medium and a chirped fiber Bragg grating (cFBG) as a dispersive element. The operation of the AKSS is based on dispersion mode-locking technique. Mode-locking is achieved by modulating a Sumitomo Osaka Cement Co. 14-GHz fiber Mach–Zehnder intensity modulator (FMZIM) in the cavity. The modulator's pigtails consist of polarization-maintaining single-mode fibers (PMF). All other fiber connections are implemented using non-polarization-maintaining single-mode fibers. To maximize transmission in the cavity, inline polarization controllers (PC) are employed. Output light is extracted via a directional coupler (DC) with 80% of power reinjected into the cavity.

As a gain medium, a CIP Technologies SOA with 3-dB bandwidth of 60 nm and central wavelength 1525 nm at a current of 100 mA is employed. The SOA is driven and controlled by a Thorlabs laser diode controller and a Thorlabs temperature controller. The SOA is followed by a polarization-insensitive optical isolator (FOCI Inc.), ISO, and by an SMF-28e delay of approximately 200 m in length. An optical circulator (AFW Technologies), CIRC, conveys the light to a chirped fiber Bragg grating (VFibre), cFBG. The cFBG exhibits 40-nm spectral bandwidth and chromatic anomalous dispersion of 10 ps/nm.

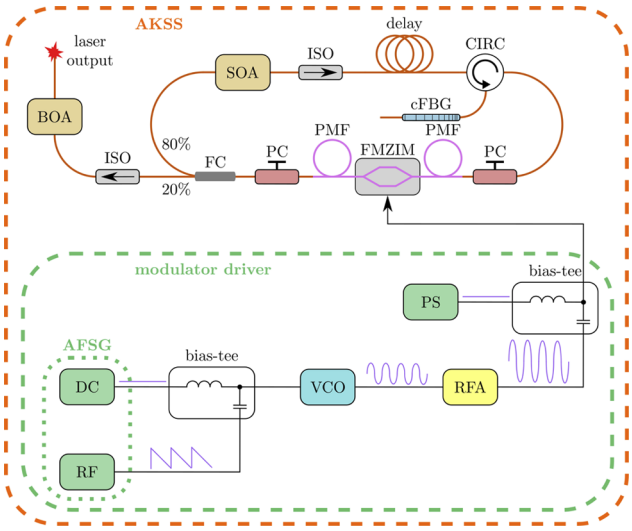

Fig. 1. AKSS setup. SOA, semiconductor optical amplifier; ISO, optical isolator; CIRC, optical circulator; cFBG, chirped fiber Bragg grating; PC, polarization controller; FMZIM, fiber Mach–Zehnder intensity modulator; PMF, polarization-maintaining fiber; FC, fiber coupler; BOA, booster amplifier; AFSG, arbitrary function signal generator; VCO, voltage-controlled oscillator; RFA, RF amplifier; PS, power supply.

The ISO together with the CIRC ensure unidirectional lasing in the laser cavity. The total cavity round trip length was evaluated as 226 m. After isolation, the laser cavity output is amplified with a booster amplifier (CIP Technologies), BOA.

A schematic diagram of the electronic circuitry driving the modulator is detailed in Fig. 1 as well (inside the green dashed rectangle). A voltage-controlled oscillator (Mini-Circuits Inc.), VCO, is driven by a ramp signal from an Agilent Technologies arbitrary function signal generator, AFSG, through an in-house bias-tee. The VCO output signal is amplified by a Mini-Circuits radio frequency (RF) amplifier, RFA, and then applied to the intensity modulator through a high-frequency bias-tee. The operating point of the modulator is controlled separately by DC voltage from a regulated power supply, PS.

For lasing characterization of the AKSS, the laser output is connected to an interferometer whose scheme is depicted in Fig. 2. The interferometer consists of two couplers with recirculation of the reference wave to avoid light being directed back into the optical source and terminated with a balanced photodetector (Thorlabs 200 MHz), bPhD. The signal from the bPhD was observed on an RF spectrum analyzer, RFSA, and oscilloscope, OSC.

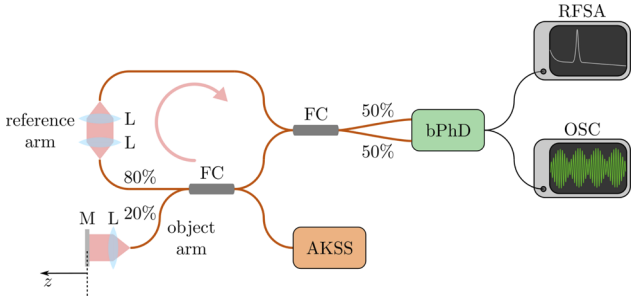

Fig. 2. SS-OCT setup used for characterization of the AKSS in Fig. 1. The recirculation of the reference wave is depicted with an arrow. AKSS, akinetic swept source system; BOA, booster optical amplifier; FC, fiber coupler; L, launcher lens system; M, mirror; bPhD, balanced photodetector; RFSA, RF spectrum analyzer; OSC, oscilloscope.

To mode-lock the laser, the modulation frequency f_m of the signal applied to the FMZIM must match an integer number m of the fundamental resonant frequency of the laser cavity (free spectral range of the cavity), $f_r(\lambda)$, [14]:

$$f_m(\lambda) = m f_r(\lambda) = \frac{mc}{n(\lambda)L_{round}(\lambda)} = \frac{mc}{n(\lambda)(L_{cav} + 2L_g(\lambda))}, \quad (1)$$

where c is the speed of light in a vacuum, $L_{round}(\lambda)$ is the cavity round trip length, $n(\lambda)$ is the effective group index of refraction of the fiber in the cavity, L_{cav} is the cavity fiber length, and $L_g(\lambda)$ is the penetration depth of the wave of wavelength λ in the cFBG. The chromatic dispersion in the laser cavity due to the fiber and cFBG is indicated by the wavelength λ dependence of n and L_g in Eq. (1), respectively.

Two tuning regimes are possible. In a first regime, the change in the modulation frequency $\Delta f_m = |f_m(\lambda_1) - f_m(\lambda_0)|$ to tune the lasing wavelength is smaller than the resonant frequency $\bar{f}_r$. This is similar to previous reports from all other groups [10,11,14]; therefore, we will refer to this operational regime as a conventional dispersive cavity tuning modality. In this case, there is a single resonance condition involved, that of mode-locking by a signal with the modulation frequency multiple of the inverse of the cavity round trip, as indicated in Eq. (1). A second regime, which is employed here, is when in addition to the first resonance condition, the sweep frequency f_s is close to the fundamental resonant frequency $\bar{f}_r$ of the cavity. This allows operation at much larger sweeping frequencies that can be controlled by the cavity length [see Eq. (1)]. We refer to this regime as a dual resonance dispersive cavity tuning modality. As explained further below, in this case, Δf_m is several times larger than $\bar{f}_r$. To distinguish between the first and the second regime, we will label the parameters involved using one of the two subscripts *single* or *dual*, respectively. The wavelength tuning range in the first regime is given by [10,11]

$$\Delta\lambda_{single}(\Delta f_m) = |S_{single}|\Delta f_m = \left|\frac{1}{\mathrm{TDD}_{round}\bar{f}_r f_{m0}}\right|\Delta f_m, \quad (2)$$

where $f_{m0} \equiv f_m(\lambda_0)$, $\mathrm{TDD}_{round} = D_{cav}L_{cav} + \mathrm{TDD}_g$ is the effective time delay dispersion of the light traveling a round trip through the laser cavity, TDD_g is the time delay dispersion due to the cFBG, whereas D_{cav} is the effective dispersion coefficient due to the fiber only and other optical parts in the cavity. The proportional constant S_{single} in Eq. (2) is the so-called wavelength tuning sensitivity.

Dual resonance sweeping regime. A negative ramp signal with DC offset of 5 V, peak-to-peak amplitude of 10 V, and reference frequency $f_{s0} = 912$ kHz is applied to the VCO. The negative direction of the ramp function is used, as it was noticed that better coherence properties are achieved than when using a positive ramp. For the sign of dispersion in the cavity (anomalous), this determines tuning from a short to a long wavelength region (forward sweeping) [11]. An experimentally recorded RF spectrum of the VCO output signal is displayed in Fig. 3. The spectrum consists of a frequency comb with repetition f_{s0} and bandwidth approximately given by $\Delta f_m \approx N_{RF} f_{s0} \doteq 185$ MHz, where N_{RF} is here defined as the

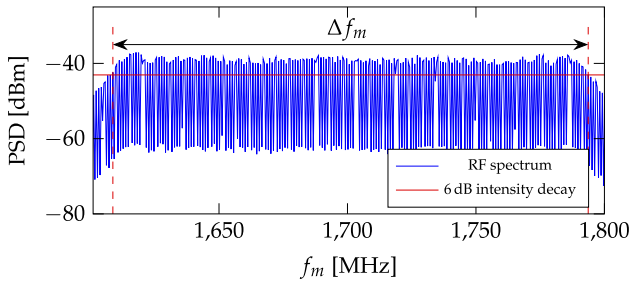

Fig. 3. Experimentally recorded RF spectrum at the output of the VCO swept at $f_{s0} = 912$ kHz over $\Delta f_m \doteq 185$ MHz giving a number of frequency components $N_{RF} \gtrsim 200$. PSD, power spectral density.

number of frequency components of the comb of whose intensity decays by less than 6 dB.

For convenience, let us consider the sweep frequency f_s written as

$$f_s = f_{s0} + \delta f_s = f_r(\lambda_0) + \delta f_s, \tag{3}$$

where $f_r(\lambda_0) = f_{s0}$ is the resonant frequency for the lasing wavelength λ_0 and δf_s is the frequency detuning from $f_r(\lambda_0)$ that could assume both positive and negative values. The frequency components of the comb in Fig. 3 can be then written in the general form as

$$f_m(\lambda) = f_{m0} + p[f_r(\lambda_0) + \delta f_s], \tag{4}$$

where p is an integer going through the set of values: $(1 - N_{RF})/2, \ldots, -1, 0, 1, \ldots, (N_{RF} - 1)/2$. For no detuning, when $\delta f_s = 0$, the comb in Fig. 3 consists of components $\ldots, f_{m0} - f_r(\lambda_0), f_{m0}, f_{m0} + f_r(\lambda_0), \ldots$ made of multiples of the fundamental resonant frequency $f_r(\lambda_0)$ only. If this signal is applied to the modulator, any component determines the same single lasing wavelength λ_0 emitted, as shown in Fig. 4(a) for an example of just three RF components. This happens because each of the components is at the center of the RF tuning bands illustrated by the small rectangles at the bottom of the sketches in Fig. 4. These bands are repeated at f_s and their width is $\Delta f_b \leq \bar{f}_r$.

The only way to obtain wavelength tuning is to detune f_s from $f_r(\lambda_0)$ in Eq. (3). When $\delta f_s \neq 0$, the RF comb in Fig. 3 consists of components $\ldots, f_{m0} - f_r(\lambda_0) - \delta f_s, f_{m0}, f_{m0} + f_r(\lambda_0) + \delta f_s, \ldots$ made of multiples of different fundamental resonant frequencies $f_r(\lambda)$, deviated by δf_s from one RF tuning band to the next. The principle of lasing when $\delta f_s \neq 0$ for the example of just three lasing wavelengths λ_{-1}, λ_0, λ_1 is displayed in Fig. 4(b) [15]. The wavelengths λ_{-1}, λ_0, λ_1 are generated by RF components $f_{m0} - f_r(\lambda_0) - \delta f_s, f_{m0}, f_{m0} + f_r(\lambda_0) + \delta f_s$, respectively, as given by Eq. (1). Assuming N_{RF} frequency components and that S_{single} in Eq. (2) is approximately constant over Δf_m, the wavelength tuning

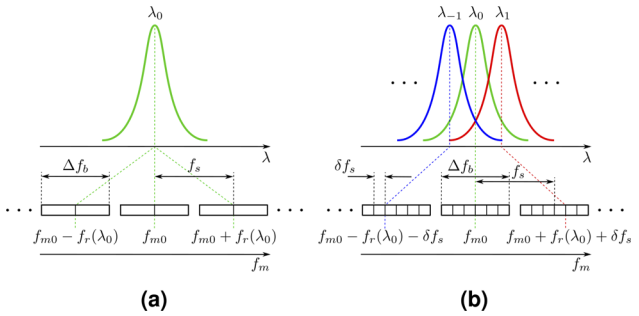

Fig. 4. Tuning principle of the AKSS when employing a dual resonance regime: (a) $\delta f_s = 0$; (b) $\delta f_s \neq 0$.

range $\Delta\lambda_{dual}$ in the dual resonance regime can be estimated as

$$\Delta\lambda_{dual}(\delta f_s) = S_{dual}|\delta f_s| = N_{RF}|S_{single}||\delta f_s| \approx \frac{\Delta f_m}{f_s}|S_{single}||\delta f_s|, \tag{5}$$

where S_{dual} is the wavelength tuning sensitivity in the dual resonance regime. Equation (5) shows that $\Delta\lambda_{dual}$ increases approximately linearly with δf_s.

The dependence of laser coherence on the detuning δf_s can be assessed by defining a number of RF tuning bands per optical spectral line $N_{\delta\lambda}$ calculated by

$$N_{\delta\lambda}(\delta f_s) = \frac{N_{RF}}{N_{\Delta\lambda}} \approx \frac{\Delta f_m}{f_s}\frac{\delta\lambda_{st}}{\Delta\lambda_{dual}(\delta f_s)}, \tag{6}$$

where $N_{\Delta\lambda} = \Delta\lambda_{dual}(\delta f_s)/\delta\lambda_{st}$ is the number of distinct optical spectral lines within the tuning range $\Delta\lambda_{dual}(\delta f_s)$ and $\delta\lambda_{st} \doteq 0.13$ nm is the linewidth measured in the static regime. If $N_{\delta\lambda} < 1$, degradation of laser coherence properties are expected.

The optical peak-hold spectra obtained without the BOA for different values of the detuning frequencies δf_s from 912 kHz are depicted in Fig. 5. To obtain flat optical spectral shapes, the polarization state was altered by fine adjustments applied to the PCs in Fig. 1. The right vertical axis in Fig. 6 shows FWHM tuning range against detuning δf_s. According to the experimental results in Fig. 6, $\Delta\lambda_{dual}(\delta f_s)$ exhibits a tuning sensitivity $S_{dual} \doteq 9$ nm/kHz down to $\delta f_s = -2.8$ kHz. The laser output power dependence against δf_s without BOA is shown in Fig. 6 on the left vertical axis. The drop in the output power with δf_s can be associated with the decrease of effective number of round trips of the photons circulating in the cavity [4,16].

Employing the BOA at the cavity output, the output power increases to 6.9 mW. The roll-off measurements are obtained in Fig. 7 using the interferometer sketched in Fig. 2. For $\delta f_s = -1.6$ kHz, -2.2 kHz, and -2.8 kHz, for which tuning ranges of 15 nm, 20 nm, and 25 nm are achieved, respectively, similar decays of sensitivity are observed with optical path difference

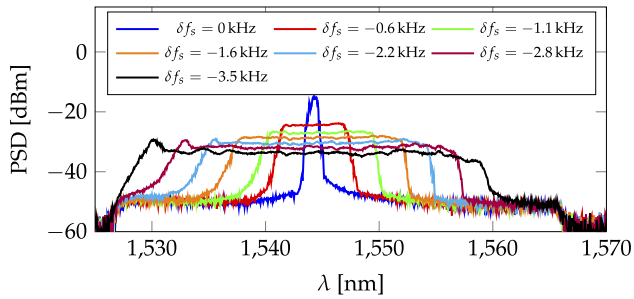

Fig. 5. Measured peak-hold spectra when employing a dual resonance regime. PSD, power spectral density.

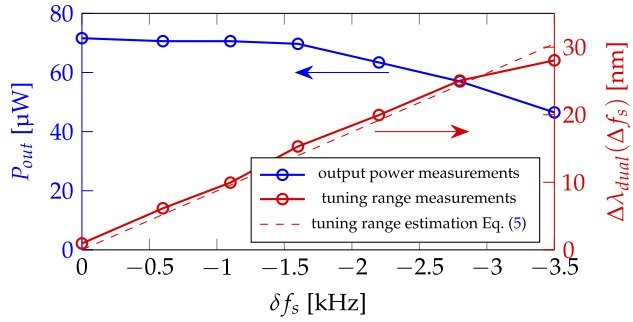

Fig. 6. Output power values P_{out} (left) and tuning ranges λ_{dual} (right) measured without the booster.

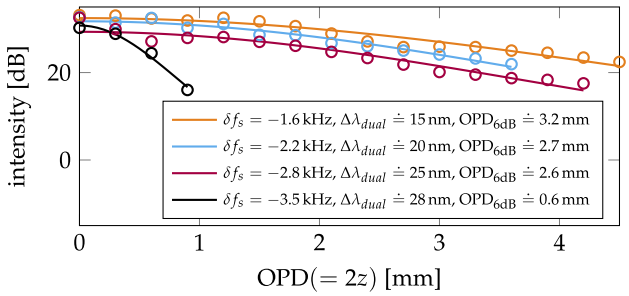

Fig. 7. Axial point spread profiles at 1 mm for different tuning ranges. For better display, the profiles are normalized and aligned at $z = 1$ mm.

Table 1. Comparison of the Measured Axial Resolution Values δz in Fig. 7 with the Theoretical Calculations δz_{t-h} Obtained for a Top-Hat Optical Spectral Shape

$\Delta\lambda_{dual}$ [nm]	10	15	20	25
δz [mm]	0.13	0.10	0.08	0.06
δz_{t-h} [mm]	0.14	0.10	0.07	0.06

(OPD) over 2 mm. For $\delta f_s = -3.5$ kHz, degradation of coherence is observed. Using Eq. (6) for $|\delta f_s| \leq 2.8$ kHz, $N_{\delta\lambda}(\delta f_s) > 1$, while for $|\delta f_s| = 3.5$ kHz, $N_{\delta\lambda}(\delta f_s) \doteq 0.88$, which explains the quicker decay in sensitivity with OPD for this detuning.

Sensitivity η obtained from the interferometer is measured for an OPD value close to zero and is calculated as $\eta = 20\log(A_{OPD}/A_{floor})$, where A_{OPD} and A_{floor} represent peak amplitude and floor level, respectively. The noise level is measured when the object signal is obstructed and at the same frequency as that of the peak. A sensitivity of 66 dB without the BOA is obtained. By adding the BOA, the sensitivity at the same OPD value increases to 82 dB.

To measure the axial resolution, correction is necessary for the chirp in the optical spectrum output modulation, due to nonlinear sweeping and due to dispersion in the interferometer. To this goal, the method of master-slave interferometry [17] is used. Axial point spread functions for different tuning ranges in Fig. 8 are produced at $z = 1$ mm. In Table 1, the measured axial resolution values δz measured at FWHM are compared with the theoretical $\delta z_{t-h} \approx 0.60\lambda^2/\Delta\lambda$ calculated for a top-hat optical spectral shape [18]. The measured resolution values are in good agreement with the theoretical calculations.

Conclusion. In this paper, the feasibility of employing the dual resonance sweeping regime in a swept source OCT at 1550 nm using an intensity modulator is presented for the first time. A tuning bandwidth of 25 nm at a sweep rate of ≈ 900 kHz is obtained. Better sensitivity decay with OPD of 2.6 mm at 6 dB is obtained than 0.75 mm reported in [13] for an even smaller tuning range of 10 nm only. The wavelength tuning range achievable in the dual resonance regime is restricted by the modulation frequency range available and by the coherence properties degradation. A rather slow decay in power with wavelength tuning range is observed. The relatively low output power is due to the mix of PM fiber components with non-PM fiber components in the laser cavity and due to the low power SOA available in the study. We believe that by assembling a laser cavity equipped with a higher gain and more powerful SOA and using only PM fiber components, substantially higher output power may become possible.

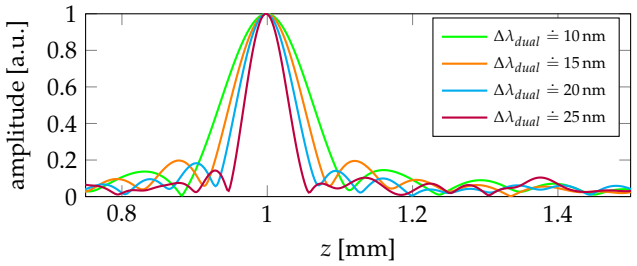

Fig. 8. Axial point spread profiles at 1 mm for different tuning ranges. For better display, the profiles are normalized and aligned at $z = 1$ mm.

Funding. HORIZON EUROPE Marie Sklodowska-Curie Actions (860807).

Acknowledgments. R.R. and A.P. acknowledge the EC support for NETLAS ITN, grant agreement No 860807.

Disclosures. A.P. and A.B. are co-inventors of patents US 10,760,893 and US 9,383,187 and A.P. of the patent US 10,211,594. All patents are in the name of the University of Kent.

Data availability. Data underlying the results presented in this paper are not publicly available at this time but may be obtained from the authors upon reasonable request.

REFERENCES

1. A. Al-Mujaini, U. Wali, and S. Azeem, Oman Med. J. **28**, 86 (2013).
2. J. Fujimoto and W. Drexler, *Optical Coherence Tomography: Technology and Applications* (Springer, 2008).
3. T. Klein and R. Huber, Biomed. Opt. Express **8**, 828 (2017).
4. R. Huber, M. Wojtkowski, and J. G. Fujimoto, Opt. Express **14**, 3225 (2006).
5. R. Huber, D. C. Adler, and J. G. Fujimoto, Opt. Lett. **31**, 2975 (2006).
6. S. H. Yun, C. Boudoux, G. J. Tearney, and B. E. Bouma, Opt. Lett. **28**, 1981 (2003).
7. B. Potsaid, V. Jayaraman, J. G. Fujimoto, J. Jiang, P. J. S. Heim, and A. E. Cable, Proc. SPIE **8213**, 82130M (2012).
8. Z. Chen, M. Liu, M. Minneman, L. Ginner, E. Hoover, H. Sattmann, M. Bonesi, W. Drexler, and R. A. Leitgeb, Biomed. Opt. Express **7**, 3032 (2016).
9. M. Salas, M. Augustin, F. Felberer, A. Wartak, M. Laslandes, L. Ginner, M. Niederleithner, J. Ensher, M. P. Minneman, R. A. Leitgeb, W. Drexler, X. Levecq, U. Schmidt-Erfurth, and M. Pircher, Biomed. Opt. Express **9**, 1871 (2018).
10. S. Yamashita and Y. W. Takubo, Photonic Sens. **3**, 320 (2013).
11. H. D. Lee, G. H. Kim, J. G. Shin, B. Lee, C.-S. Kim, and T. J. Eom, Sci. Rep. **8**, 17660 (2018).
12. F. Toadere, R.-F. Stancu, W. Poon, D. Schultz, and A. Podoleanu, IEEE Photonics Technol. Lett. **29**, 933 (2017).
13. R. F. Stancu and A. G. Podoleanu, Opt. Lett. **40**, 1322 (2015).
14. A. Takada, M. Fujino, and S. Nagano, Opt. Express **20**, 4753 (2012).
15. A. Podoleanu and R.-F. Stancu, "Akinetic swept laser apparatus and method for fast sweeping of the same,"U.S. Patent 10, 211, 594 B2 (19February2019).
16. R. Huber, M. Wojtkowski, K. Taira, J. G. Fujimoto, and K. Hsu, Opt. Express **13**, 3513 (2005).
17. A. G. Podoleanu and A. Bradu, Opt. Express **21**, 19324 (2013).
18. J. P. Fingler, "Motion contrast using optical coherence tomography," Ph.D. thesis (California Institute of Technology, 2007).